Materials Today 91 (2025) 244–252

Contents lists available at ScienceDirect

Materials Today

journal homepage: www.elsevier.com/locate/mattod

Scalable low-emissivity and RF-transparent dielectric coatings for year-round energy-saving buildings under all weather conditions

Yi Zhang [a,1], Senji Li [a,1], Yucan Peng [b], Chenglong She [a], Minghao Dong [a], Keqiao Li [c], Fan Yang [a], Weiying Hou [d], Han Gao [a], Chenshu Wu [d], Baoling Huang [c], Jiawei Zhou [a], Philip C.Y. Chow [a,*], Xiaobo Yin [a,e,*]

[a] Department of Mechanical Engineering, The University of Hong Kong, Hong Kong, China
[b] Department of Energy and Resources Engineering, College of Engineering, Peking University, Beijing, China
[c] Department of Mechanical and Aerospace Engineering, The Hong Kong University of Science and Technology, Clear Water Bay, Kowloon, Hong Kong, China
[d] Department of Computer Science, The University of Hong Kong, Hong Kong, China
[e] Department of Physics, The University of Hong Kong, Hong Kong, China

ARTICLE INFO

Keywords:
Energy-saving buildings
Low-emissivity
Multiple light scattering
Thermal radiation
Ceramic-polymer coatings

ABSTRACT

Low-emissivity (low-E) materials are crucial for building energy efficiency, but all conventional solutions rely on electrically conductive materials that severely block wireless communication, posing a critical obstacle for smart city infrastructure. Here, we present a simple and scalable polymer-ceramic composite (LE-PCC) that breaks this long-standing trade-off. Composed of zinc sulfide (ZnS) microparticles and polyethylene (PE) binders with tailored microporosity, our LE-PCC achieves a high mid-infrared reflectance (0.68). Unlike existing low-E materials, which rely on free electrons to reflect thermal radiation, LE-PCC operates through enhanced backscattering of mid-infrared light by multiple scatterings in a disordered dielectric medium. LE-PCC significantly outperforms conventional low-E materials in telecommunication signal transmission, reducing attenuation to 2.5 dB (vs. 15 to 70 dB for conventional low-E materials). Furthermore, incorporating infrared-transparent pigments allows for customizable coloring without compromising mid-infrared reflectance, broadening its architectural versatility. Building energy simulations reveal that white and colored LE-PCCs are effective in different climates, such as Hong Kong (46.33 GJ savings) and Los Angeles (43.59 GJ savings), for a midrise apartment annually. Combining thermal insulation, wireless transparency, architectural adaptability, and low-cost, scalable fabrication, LE-PCC emerges as a new class of photonic coatings and a transformative solution for energy-efficient and IoT-enabled smart cities.

Introduction

Buildings contribute approximately 30 % of global energy consumption and are responsible for 26 % of energy-related greenhouse gas emissions. A significant portion of this energy—up to 45 % in some cases—is consumed in heating and cooling indoor spaces [1–4] As the world intensifies efforts to reduce carbon emissions, enhancing the energy efficiency of buildings has emerged as a critical priority. Passive radiative cooling technologies can dissipate heat to the cold universe through the atmospheric window (~8–13 μm) [5–8]. However, radiative cooling can only save cooling energy. Low-emissivity (low-E) materials on the other hand can minimize heat exchange between indoor and outdoor environments and save both cooling and heating energy [9–15]. By reflecting infrared (IR) thermal radiation, these materials help retain heat during winter and block external heat during summer [16–18].

Current low-E technologies solely rely on electrically conductive materials such as metals [9,19], conductive metal oxides [20], conductive polymers [21,22], and conductive metal carbides and ceramics [23,24]. The underlying mechanism is metallic free-electron reflection, which can be described as follows: the absorbed light induces alternating electrical currents on the conducting surface of these materials, which, in turn, promptly reemit the light, resulting in strong reflectivity. While these materials effectively reflect thermal radiation,

* Corresponding authors..
E-mail addresses: pcyc@hku.hk (P.C.Y. Chow), xbyin@hku.hk (X. Yin).
[1] Y.Z and S.L contributed equally to this work.

https://doi.org/10.1016/j.mattod.2025.10.014
Received 2 June 2025; Received in revised form 14 August 2025; Accepted 6 October 2025
Available online 13 October 2025

their high electrical conductivity significantly attenuates radio frequency (RF) signals. This causes indoor telecommunication blocking, a challenge that becomes increasingly critical as smart cities rely more heavily on seamless wireless connectivity (*e.g.*, GSM, GPS, Wi-Fi, 3G, 4G, 5G signals [25–27], and emerging 6G technologies [28–30]). Although signal boosters can mitigate this issue, they introduce additional costs, consume energy, and contribute to e-waste. Hence, there is an urgent need for low-E materials that combine high IR reflectivity with transparency to wireless signals. Conventional strategies, such as frequency-selective surfaces (FSS), offer potential solutions but are limited by their narrow transmission bandwidths and high fabrication costs [31–33].

To address this challenge, we introduce a low-E polymer-ceramic composite (LE-PCC) that achieves both low thermal emissivity and high telecommunication transparency (Fig. 1a). This innovative material is designed by embedding IR-transparent ceramic microparticles into an IR-transparent polymer matrix, forming a structure that effectively scatters and reflects thermal radiation across a broad wavelength range (Fig. 1b). LE-PCC coatings demonstrate a mid-IR reflectance of 0.68, significantly surpassing that of commercial white paints with (0.04), enabling efficient wireless signal transmission (Fig. 1c). Additionally, the coatings are scalable, mechanically robust, and compatible with various substrates, providing a practical and sustainable solution for next-generation smart buildings.

Results

Design of low-E polymer-ceramic composite (LE-PCC)

When an electromagnetic wave propagates through a heterogeneous medium, it experiences multiple scattering [34–38]. Scattering involves the redirection of the incident energy into different directions around the particle. In the case of multiple scatterings within a heterogeneous medium, the presence of additional particles along the path of the incident beam leads to an increase in both absorbed and scattered radiation. If the medium is relatively transparent, light can penetrate deeper, enabling more scattering events without significant absorption by the particles. The scattering behavior of particles is influenced by factors such as particle size, volume fraction, and the wavelength of the incident light. This is why snow appears white, as ice crystals scatter light multiple times. Similarly, the principle of multiple scattering of particles with sizes comparable to the wavelength of interest is utilized to construct LE-PCC. In order to minimize the absorption, the constructing components should be transparent in the IR. Common IR-transparent materials, as outlined in Table S1, include silicon, germanium, halides (*e.g.*, NaCl, CaF_2, BaF_2, KBr), diamond, polyethylene (PE), III-V family compound semiconductors (*e.g.*, GaAs), and II-VI family compound semiconductors (*e.g.*, ZnSe, CdTe, ZnS). Zinc sulfide (ZnS) was selected as the primary material for constructing the LE-PCC for several reasons: (1) it is transparent in a larger IR range (up to 14 μm); (2) it is electrically insulating; (3) it is insoluble in water and chemically inert in ambient environments; (4) it possesses a higher refractive index compared to other IR-transparent materials, which enhances its scattering capability; (5) it is abundant on Earth, primarily found as the mineral Sphalerite, and is thus cost-effective. Compressing and sintering ZnS powders does not yield a solid structure, as ZnS does not sinter as readily as aluminium oxide or silica. Drawing inspiration from ceramic coating fabrication [39–41], which incorporates ceramic particles within an organic binder, we also use a binder to connect ZnS particles. PE is an ideal candidate for the binder because PE is highly transparent in the IR range (only consists of C–C and C–H bonds). The spectrum of PE is shown in Fig. S3. Hence, adding PE as a binder does not influence the IR reflectance of the whole composite. Besides, PE has a low softening temperature (~120 ℃), which can easily melt and solidify to bind the ZnS particles. The resulting LE-PCC structure comprises three key components: (i) ZnS particles with sizes comparable to the IR wavelengths to induce strong scattering, (ii) PE as the binder to glue ZnS particles together and provide refractive index contrast for light scattering at ZnS/PE interfaces, and (iii) Air voids to provide a larger refractive index contrast for stronger scattering effects. Fig. 2a shows the optical constants of the three main components. The shaded areas in yellow and blue represent the solar intensity and the blackbody thermal emission at 300 K, respectively. Both ZnS and PE have low absorption

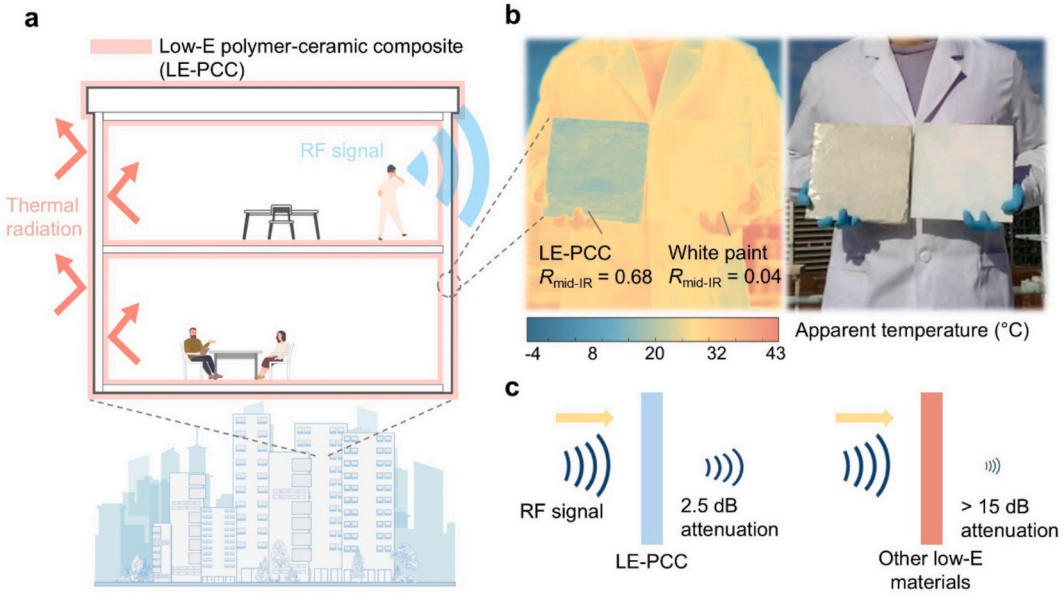

Fig. 1. Concept illustration of low-E polymer-ceramic composite (LE-PCC). (**a**) Schematic illustration showing the potential effects of our non-metallic LE-PCC on building exterior walls, interior walls, and roofs, which can reflect infrared radiation to provide thermal radiation insulation without causing attenuation of telecommunication signals. (**b**) Thermal infrared (left) and visible (right) camera images of our LE-PCC and conventional white paint, both 20 cm by 20 cm. While both samples have similar solar reflectivity and appear white, our LE-PCC shows significantly lower thermal emissivity (higher reflectance of thermal infrared radiation) than conventional white paint. (**c**) The signal attenuation rate of our LE-PCC and other existing low-E materials. LE-PCC only attenuates RF signal by 2.5 dB, while other low-E materials attenuate more than 15 dB. These results are from the experiments in the following content.

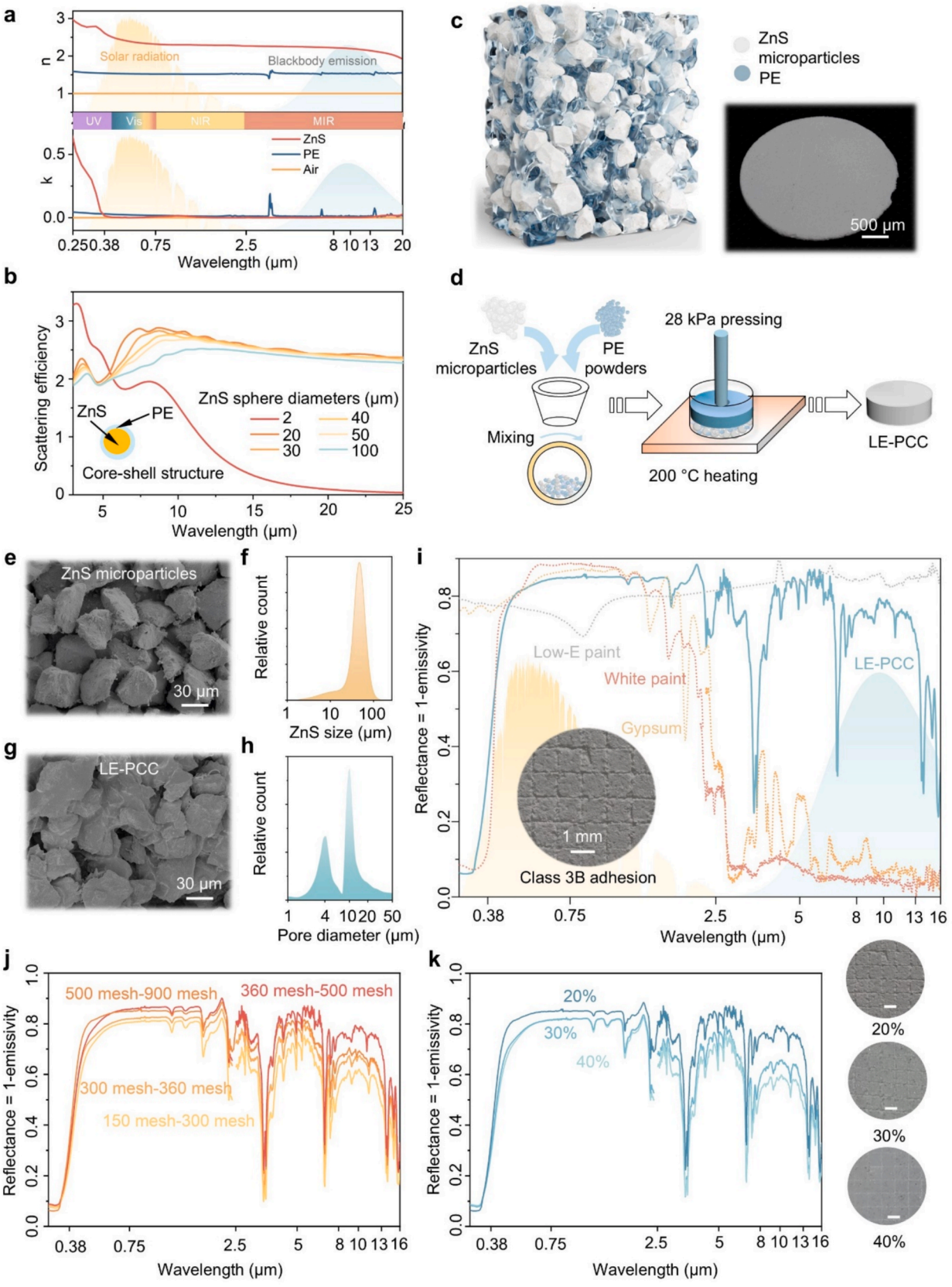

(caption on next page)

Fig. 2. Optical and structural characterizations of LE-PCC. (**a**) Refractive index (n) and extinction coefficient (k) of ZnS, polyethylene (PE), and air. The combination of large refractive index differences and low extinction coefficient spanning from ultraviolet to mid-infrared between these materials causes effective and broadband light scattering. The regions shaded in orange and red depict the solar intensity and blackbody thermal emission at 300 K. (**b**) The calculated scattering efficiency of a core–shell structure, with ZnS as the core and PE as the shell (1 μm thick), was analyzed. According to the results, the optimal ZnS particle size ranges from 20 to 100 μm to achieve high scattering efficiency in the thermal emission range at ambient temperature, which peaks at 10 μm. (**c**) The LE-PCC features a porous structure (porosity: ~9.6 %) in which randomly arranged ZnS microparticles are bonded by PE (as a binder) to form a framework. The figure on the right shows the photograph of the LE-PCC. (**d**) Schematic illustration of the fabrication process for LE-PCC. (**e**) SEM images of the ZnS sequentially sieved by 360 mesh and 500 mesh. (**f**) The size distribution of the ZnS microparticles sequentially sieved by 360 mesh and 500 mesh. (**g**) SEM images of the LE-PCC. It can be seen that the individual ZnS microparticles are connected together by PE. (**h**) The size distribution of the pores of LE-PCC is measured by mercury porosimetry. (**i**) The measured solar reflectance and infrared emissivity of the LE-PCC. The LE-PCC has R_{solar} and $R_{mid\text{-}IR}$ of 0.81 and 0.68, respectively. The spectra for gypsum and white paint are also shown here. For gypsum, $R_{solar} = 0.84$; $R_{mid\text{-}IR} = 0.08$; For white paint, $R_{solar} = 0.82$, $R_{mid\text{-}IR} = 0.04$. All three materials have similar R_{solar}. In contrast, LE-PCC processes high $R_{mid\text{-}IR}$, while the other two have low $R_{mid\text{-}IR}$ below 10 %. The spectra of conventional low-E aluminium paint are also shown. The appearance of the LE-PCC is very similar to that of gypsum. The inside figure shows the LE-PCC undergoing a standard cross-cut tape test (ASTM D3359-2). The area of the coating that was removed was 5–15 %, demonstrating a Class 3B adhesion strength. Parameters study of ZnS particle size and PE fraction. (**j**) ZnS microparticles with 4 different size ranges were used for constructing LE-PCC. They are 1) particles sieved by 150 mesh and 300 mesh; 2) particles sieved by 300 mesh and 360 mesh; 3) particles sieved by 360 mesh and 500 mesh; and 4) particles sieved by 500 mesh and 900 mesh. (**k**) The PE fraction was determined based on the weights of the ZnS and PE particles. The sample with a PE volume fraction of less than 20 % failed to form a solid structure due to insufficient binder content. The figure on the right shows the cross-cut tape test for samples with different PE fractions. The scale bar is 1 mm.

extinction coefficients in the IR. Furthermore, ZnS, with its high refractive index in the IR, facilitates efficient scattering in the IR when embedded in PE and air. This can be demonstrated in a simple photonic theoretical model, where a ZnS microsphere is wrapped by a PE shell with 1 μm thickness. The scattering properties of particles depend on their relative size with respect to incoming radiation and show different characteristics according to their size and shape distribution. As shown in Fig. 2b, ZnS spheres with 20–100 μm diameters have high scattering efficiency over the MIR range.

Fig. 2c illustrates the structure of LE-PCC, which consists of discrete ZnS microparticles interconnected by a PE matrix. We fabricated the LE-PCC using a facile manufacturing process which is well-suited for mass production, as illustrated in Fig. 2d. Firstly, ZnS crystals were mechanically ground into particles and then sequentially sieved by different combinations of mechanical meshes to obtain different size ranges (Fig. S1). Mesh size is often used in industry and refers to the number of openings per linear inch of a sieve screen. The relationship between mesh and particle diameter can be obtained from the Table S2. The ZnS microparticles sequentially sieved by 360 mesh sieve and 500 mesh sieve allowed us to obtain particles with 20–100 μm diameters, with a peak distribution at ~ 40 μm (Figs. 2e, f). These ZnS microparticles were then mixed with polyethylene (PE) microparticles (mean diameter: 13 μm, Fig. S2) at a mass ratio of 5:1, corresponding to a PE volume fraction of 20 %. Afterward, the mixture was heated in an oven at 200 ℃ under applied pressure (28 kPa) for 10 min to form the porous LE-PCC. With a low softening temperature (~120 ℃) and high IR transmittance, PE particles act as a nonconventional binder, creating a robust porous framework. During heating, the PE particles melt and conform to the surface of the ZnS microparticles. As the temperature returns to ambient, the solidified PE connects the ZnS particles, forming a rigid solid. In addition, due to the limited amount of PE, micrometer-sized air pores remain within the solid, as shown in Fig. 2g. The air pore size distribution of the LE-PCC prototype is shown in Fig. 2h, confirming their sizes and distribution. Pore-size measurements indicate that the pore sizes are bimodally distributed, with distributions centered at ~ 4 and ~ 10 μm.

The LE-PCC exhibits a high broadband reflectivity from solar wavelength to thermal wavelength, leading to a solar reflectance (R_{solar}) value of 0.81 and MIR reflectance ($R_{mid\text{-}IR}$) value of 0.68. For comparison, two conventional building materials, gypsum and white paint, show (R_{solar}, $R_{mid\text{-}IR}$) of (0.84, 0.08) and (0.82, 0.04), respectively (Fig. 2i). The reduction in reflectance of LE-PCC at 3.4 μm, 6.8 μm, and 13.8 μm are due to the absorption of the PE binder. Although the absorption at 3.4 μm is relatively strong, the blackbody radiation for this wavelength is small. In addition, the absorption peaks at 6.8 μm and 13.8 μm are narrow. Therefore, the average mid-infrared reflectance of the LE-PCC was maintained at 0.68. The conventional low-E paint using aluminium microflake was also shown here for comparison [9]. The $R_{mid\text{-}IR}$ of this low-E paint is 0.77. Although the number is higher than our LE-PCC, its attenuation of telecommunication signals restricts its applications in buildings, as seen in the following contents. In addition, we prove that with the $R_{mid\text{-}IR}$ of 0.68, massive energy savings can be obtained from building energy simulations using LE-PCC. The adhesion strength of the LE-PCC was tested using a standard cross-cut tape test (ASTM D3359). After the test, the area of the composite that was removed was 5 ~ 15 %, demonstrating a high adhesion strength (Class 3B).

The ZnS particle size and PE fraction were systematically adjusted to optimize the $R_{mid\text{-}IR}$, as shown in Figs. 2j and k. ZnS particles with different sizes were obtained by sieves with different mesh numbers. The particle size distributions of all four samples are shown in Fig. S5. Smaller ZnS particles scatter light at shorter wavelengths, as demonstrated theoretically in Fig. 2b. However, to achieve higher $R_{mid\text{-}IR}$ at room temperature blackbody emission, which peaks between 8–10 μm, ZnS particles sieved between 360 mesh and 500 mesh exhibited the highest reflectance in this range, which also matches our simulation results in Fig. 2b. Smaller or larger ZnS particles all decrease the reflectance in the IR range. Regarding the PE fraction, a higher PE content enhances the bonding strength between ZnS particles, as evidenced in Fig. 2k. For instance, samples with a PE fraction below 20 % fail to form a solid structure, whereas the adhesion strength of a sample with a 40 % PE fraction achieves Class 4B performance. However, excessive PE content reduces porosity, leading to diminished scattering and lower $R_{mid\text{-}IR}$. A PE volume fraction of 20 % achieves an optimal balance, enabling the formation of a mechanically robust composite with excellent $R_{mid\text{-}IR}$. The spectra of LE-PCC with different thicknesses are shown in Fig. S6. The spectra for LE-PCC with thicknesses of 2 mm and 3 mm are nearly identical, leading to the conclusion that a thickness of 2 mm is sufficient to achieve saturated solar and mid-infrared reflectance.

Thermal insulation performance

The low-emissivity property of the LE-PCC coating was first visualized using a thermal camera. The LE-PCC sample was placed on a hot plate at 100 °C. A piece of carbon tape with high thermal conductivity was affixed to the surface of the LE-PCC coating. Carbon tape and LE-PCC reached the same temperature. Despite the LE-PCC and the carbon tape having the same temperature, it is clear that the LE-PCC coating appeared much cooler, highlighting its reduced heat radiation (Fig. 3a).

To further investigate the thermal insulation performance of the LE-PCC coating, we tested building simulants in artificial hot and cold environments. We used an enclosed chamber with circulated water to

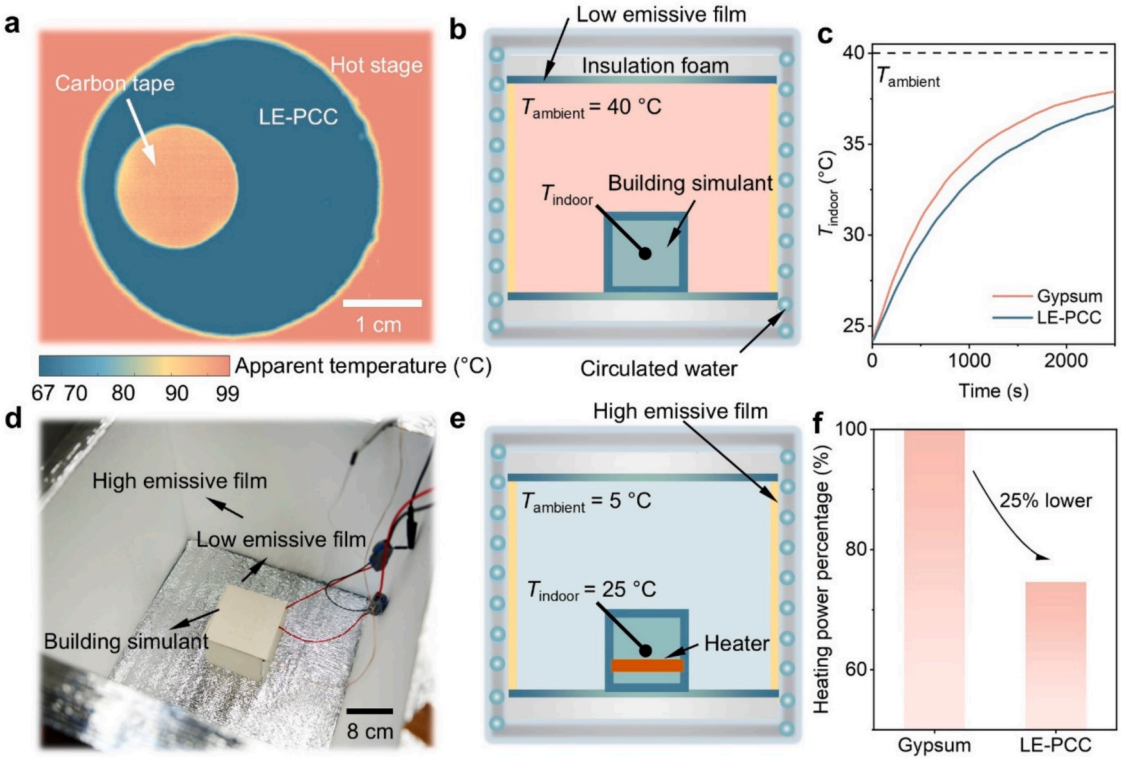

Fig. 3. Thermal insulation property of LE-PCC. (**a**) The infrared thermal image of LE-PCC on a hot plate with 100 °C and a carbon tape stuck on it. The image shows the low thermal emissivity of the LE-PCC. (**b**) Schematic illustration of the measurement apparatus for the heat gain test. A 40 ℃ ambient environment ($T_{ambient}$) was created by the circulated water system for the building simulant. Thermocouples were employed to measure the T_{indoor} curve of the building simulant. (**c**) Measured indoor temperature curves of the building simulant with different surfaces for the heat gain test. The simulant coated with LE-PCC exhibited a slower temperature increase, confirming reduced radiative heat gain. (**d**) A photograph of the heat loss measurement apparatus. (**e**) Schematic illustration of the measurement apparatus for the heat loss test. A 5 ℃ ambient environment was maintained by the circulated water system. An electric heater simulated building conditions by generating heat to keep the indoor temperature at 25°C. (**f**) Measured heating power required by the electric heater for the building simulant during the heat loss test. LE-PCC effectively reduced the necessary heating power by minimizing radiative heat loss.

create hot or cold circumstances. In these experiments, building simulants covered by LE-PCC and gypsum were measured in parallel. Thermocouples measured the inside temperature (T_{indoor}). As shown in Fig. 3b, we studied the indoor heat prevention performance in a 40 ℃ environment. The building simulant was first stabilized at room temperature (~24 ℃) and then transferred into the 40 ℃ environment with T_{indoor} recording. The temperature increase curves are valuable for comparing their ability to resist being heated. As shown in Fig. 3c, the building simulant coated with LE-PCC clearly showed a delay in temperature increase, in contrast to the simulant with gypsum. T_{indoor} was consistently lower for the simulant coated with LE-PCC before the temperature reached equilibrium. This result verifies that the LE-PCC efficiently diminished heat gain from the environment. The thermal conductivity and thermal diffusivity of LE-PCC are 0.621 W/m·K and 0.423 mm^2/s, respectively. Considering the thin thickness of the sample (2 mm) and its thermal conductivity, the insulation mechanism is primarily governed by thermal radiation rather than thermal conductivity.

We also conducted measurements for the building simulants in a cold environment (5 ℃), mimicking winter conditions (Figs. 3d and 3e). In this experiment, a Kapton electric heater was put inside each building simulant to provide heating power to maintain a constant T_{indoor} at 25 ℃. The building simulant with gypsum required 1.26 W of heating power, whereas the simulant coated with LE-PCC only needed 0.94 W. This indicates that the simulant coated with LE-PCC consumed 25 % less power (Fig. 3f). The result proves that the LE-PCC can reduce indoor heat loss in a cold environment, thus saving heating energy.

Telecommunication signal transmission

To evaluate the telecommunication signal transmission performance of various low-E materials, we first measured the dielectric spectra of LE-PCC, including the dielectric constant and dielectric loss, across two frequency ranges: 100 Hz to 2 MHz (Fig. S9) and 2 GHz to 20 GHz (Fig. 4a). And then we conducted a comprehensive experimental analysis using large samples with dimensions of 20 cm by 20 cm. The experimental setup is depicted in Fig. 4b. The experiment was done in a Radio Frequency (RF) chamber to avoid the impact of multipath reflections and ambient noises. Detailed experimental procedures are outlined in the Methods section. Fig. 4c compares the RF signal attenuation in the frequency range of 2 GHz to 18 GHz between our LE-PCC material with four conventional low-E materials, including (1) ITO on glass, (2) commercial low-E paint containing Ag, (3) Al foil, and (4) nickel/copper (Ni/Cu)-coated textiles. The LE-PCC coating used in this study maintains the same $R_{mid\text{-}IR}$ value (0.68) and thickness (≈2 mm), while the other samples have a thickness from several hundred nanometers to several hundreds of micrometers. The results clearly indicate that the conventional low-E materials show significant RF signal attenuation, ranging from 15 to 70 dB. In contrast, our LE-PCC material demonstrated superior Wi-Fi signal transmission, with only 2.5 dB attenuation. Notably, a 10 dB attenuation indicates that only one-tenth of the original power is received, signifying a substantial impact of conventional low-E materials on signal transmission. The results demonstrate that our LE-PCC can exhibit the unique combination of low-emissivity and high telecommunication signal transmission, which is an ideal property for building materials in a smart and sustainable city that demands high energy efficiency as well as seamless network coverage.

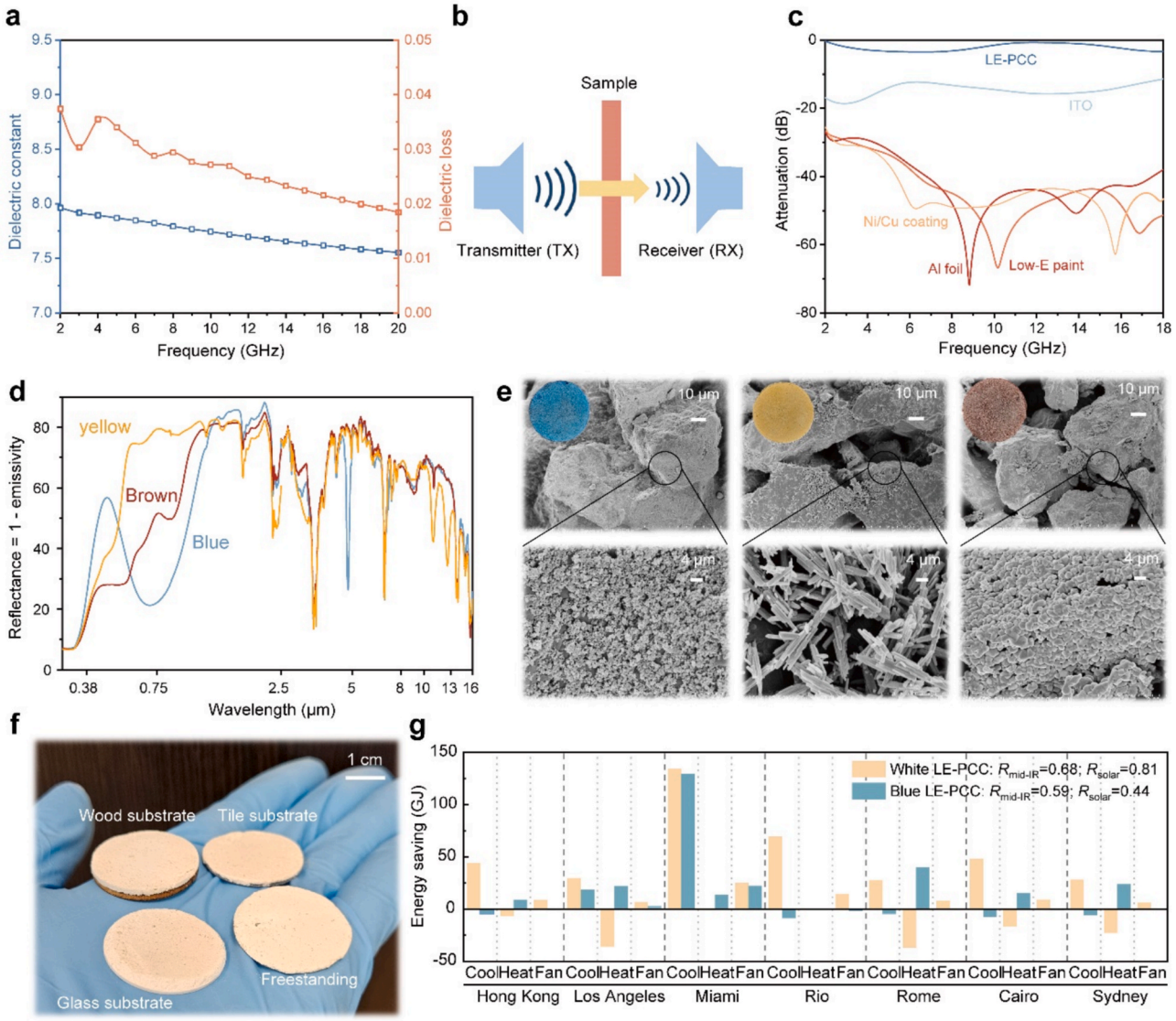

Fig. 4. The real-world application potentials of LE-PCC as a building envelope. (**a**) The dielectric spectra of LE-PCC, including dielectric constant and dielectric loss, over the frequency ranges of 2 GHz – 20 GHz. (**b**) Schematic diagram of the telecommunication signal transmission measurement setup. (**c**) The RF (2 GHz – 18 GHz) transmission attenuation of different low-E materials. LE-PCC shows the lowest attenuation. (**d**) The spectra of colored LE-PCC. The inside figure shows the photograph of colored LE-PCC. (**e**) The SEM images for colored LE-PCC. (**f**) The picture shows that the lowE ceramic can be coated on various substrates, including wood, tile, and glass, and can be freestanding. (**g**) The energy consumption simulation uses white LE-PCC, colored LE-PCC, and conventional gypsum. White LE-PCC achieves dramatic energy saving in cooling-dominated climates. Meanwhile, colored LE-PCC shows energy saving in all climates. The total HVAC consumption includes cooling, heating, and fan.

Colored LE-PCC

The LE-PCC is inherently white due to its broadband reflectance. However, colored coatings are often preferred in building applications to suit aesthetic and architectural needs. To address this, we developed various colored LE-PCCs by incorporating inorganic pigments that can selectively absorb specific portions of the visible spectrum while maintaining high transparency to the MIR range. We employed inorganic nanoparticles as pigments, specifically using Prussian blue (PB), iron oxide (Fe_2O_3), and goethite (α-FeOOH) to produce primary colors of blue, red, and yellow, respectively. These inorganic pigments are selected based on their demonstrated properties of IR transparency, non-toxicity, and cost-effectiveness, as reported in previous studies [9,11,42]. The three primary colors can be combined to produce a complete spectrum of colors. The fabrication procedure of colored LE-PCC involves first suspending inorganic nanoparticles in ethanol to create stable suspensions. These suspensions were then applied onto the white base LE-PCC via a spray coating technique to ensure uniform coverage. After the solvent evaporation, the pigment nanoparticles formed a homogenous layer on the surface. Fig. 4d displays the measured spectra of the colored LE-PCC in the primary colors, with dominant reflection wavelengths at approximately 450 nm, 600 nm, and 750 nm for blue, yellow, and red, respectively. The SEM images of the colored LE-PCC are shown in Fig. 4e. The inset figure shows the colored LE-PCC samples. The color uniformity is demonstrated by the SEM image presented in Fig. S10. Additionally, the long-term durability of the colored LE-PCC is validated and shown in Fig. S11. The R_{solar} and R_{mid-IR} of the three colored LE-PCC are shown in Table S3. Notably, the R_{mid-IR} of the colored LE-PCC remains largely unchanged despite the addition of pigments; for instance, the R_{mid-IR} of the blue low-E ceramic is 0.59, only 0.09 lower than that of the white LE-PCC. This minimal reduction is attributed to the nanoscale dimension of the inorganic pigment particles and the ultrathin (~micron-scale) nature of the coating. The signal attenuation test of colored LE-PCC is shown in

Fig. S12.

Zinc sulfide or Sphalerite is abundant and has been the principal ore mineral in the world. When composited with durable and cost-effective plastic polyethylene, the raw materials cost of LE-PCC is competitive for large-scale deployment. Furthermore, we demonstrated that the LE-PCC could be used either as a freestanding film or by coating onto various substrates, including wood, ceramic, glass, and tile, as shown in Fig. 4f. The unique combination of low-emissivity, high telecommunication signal transmission, decent adhesion strength, low cost, and versatility in terms of color and substrate make our LE-PCC material a promising solution for future coating materials in energy-efficient buildings in smart cities. The comparison of LE-PCC with the existing low-E techniques is shown in Table S3.

Energy-saving evaluation

We used EnergyPlus to evaluate the HVAC energy-saving performance of simulated cities with buildings coated with both white and colored LE-PCC. The reference building models (Post-1980 midrise apartments) defined by the US Department of Energy were adopted for simulations. The HVAC energy use (cooling, heating, fans, and water systems) was calculated for the building using conventional wall materials and walls that have the surface properties of our LE-PCC coating based on the aforementioned spectral characterizations. We chose several cities from all continents to represent different climates. As shown in Fig. 4g, the white LE-PCC can help to reduce the annual energy consumption in hot climates like Hong Kong (46.33 GJ), Miami (158.83 GJ), Rio (83.14 GJ), and Cairo (40.42 GJ). However, the high solar reflectance of the white LE-PCC, while beneficial during the summer, also results in excessive heat reflection during the winter months. This increases the heating demand in milder climates, such as Los Angeles, Rome, and Sydney, potentially offsetting the cooling energy savings achieved during summer. Consequently, this seasonal trade-off may lead to higher overall annual energy consumption in these regions. To address this limitation, we explored the use of colored LE-PCC coatings. For example, the use of blue LE-PCC can effectively decrease the amount of solar reflection, which helps to heat up the buildings during winter in addition to the thermal insulation properties enabled by the mid-infrared reflectance, thus leading to overall energy saving all year round. For example, the application of blue LE-PCC coatings enabled energy savings of 43.59 GJ in Los Angeles, 34.96 GJ in Rome, and 17.55 GJ in Sydney. The energy saving comparison of LE-PCC with the existing low-E paint is shown in Fig. S13.

Conclusion

In summary, we demonstrated a new approach for creating low-E material based on the phenomenon of multiple scatterings of light in a disordered media. The resulting electrically-insulating LE-PCC simultaneously achieves two critical functionalities: (1) high broadband reflectance for thermal radiation, which significantly reduces radiative thermal exchange for effective heat insulation, and (2) high telecommunication signal transmission (only 2.5 dB attenuation vs. 15 to 70 dB for other low-E materials), ensuring seamless network coverage. The LE-PCC prototype shows a $R_{\text{mid-IR}}$ of 0.68 and a R_{solar} of 0.81. Indoor demonstrations confirmed the thermal insulation properties of LE-PCC in winter and summer to prevent heat loss and heat gain, respectively. Colored LE-PCCs are also fabricated by adding non-toxic and abundant inorganic pigments. Using a midrise apartment model, energy-saving calculations indicate that LE-PCC coating can lead to net energy savings in many regions across the globe. In particular, we find that white LE-PCC is particularly advantageous in hot climates where space cooling is the primary need, while colored LE-PCC provides better overall energy-saving performance in moderate climates where heating is largely needed. Based on abundant raw materials and a scalable fabrication process, our LE-PCC material is inexpensive and can be applied to various existing building materials and tiles. Taken together, these attributes position LE-PCC material as a promising solution for energy-efficient buildings in future smart and sustainable cities that also demand seamless network coverage of telecommunication signals for various IoT and cloud applications. Additionally, the LE-PCC's high infrared reflectance and low RF reflectance open new possibilities for multispectral camouflage applications, further broadening its potential impact [43].

Experimental Section/Methods

Low-E polymer-ceramic composite preparation: Zinc sulfide (ZnS) crystals from Fuzhou Yinfeixun Photoelectric Technology were crushed into particles using a crusher and mechanically sieved to obtain different size ranges. ZnS and PE powders from Zhonglian Plastic were dried overnight in an oven to remove moisture. The powders were weighed in various ratios and mixed using a Vortex shaker. This mixture was applied to various substrates, including tile, wood, and glass, and then the coating was heated to 200 °C for 10 min on a hot plate to melt the PE powder. Upon cooling, the PE acted as a binder for the ZnS, forming a robust LE-PCC.

Characterizations: The MIR reflectance was assessed using a Fourier transform infrared spectrometer (Vertex, Bruker) paired with a diffuse gold integrating sphere from PIKE Technologies. Visible and NIR reflectance measurements were conducted using UV–Vis-NIR spectrometers (Cary 5000, Agilent) equipped with diffuse reflectance accessories. Scanning electron microscopy (SEM) images were captured using a Hitachi S-4800 SEM. These images were analyzed using ImageJ software. X-ray diffraction (XRD) was employed to characterize the ZnS powders and the LE-PCC. The particle size distribution of ZnS microparticles was measured by a Laser Scattering Particle Size Distribution Analyzer (Partica LA-960, Horiba). Porosity and pore distribution were measured using a mercury porosimeter (MicroActive AutoPore V 9500, Micromeritics). Infrared temperature mapping was performed with an infrared camera (Ti480 PRO, FLUKE) featuring a resolution of 640 × 480 pixels with a detection wavelength range of 7.5 to 14 μm. Thermal conductivity and thermal diffusivity were measured by laser flash analyser (LFA 467 HyperFlash, NETZSCH).

Telecommunication signal transmission: To assess the electromagnetic wave penetration of the materials, we conducted RF transmission experiments in a microwave anechoic chamber using the free-space method across the frequency range of 2 GHz to 18 GHz. A vector network analyzer (3176G, Ceyear) was utilized to connect the transmitter (TX) and receiver (RX), enabling the measurement of the Received Signal Strength Indicator (RSSI) values of the received signals. A higher RSSI value corresponds to lower signal attenuation between the TX and RX, indicating that the material exhibits minimal absorption and reflection of electromagnetic waves. The dielectric constant and dielectric loss were measured across two frequency ranges: 100 Hz to 2 MHz using a precision LCR meter (E4980AL, Keysight) and 2 GHz to 20 GHz using a vector network analyzer (N5224A, Keysight).

Heat insulation performance demonstration: The temperature-regulated chamber is made of aluminium alloy. The four sidewalls were embedded with copper tubes to circulate water inside them. A circulated water system controlled the chamber's wall temperature. Both the exterior walls of the chamber were insulated by insulation foam. The top and bottom walls were insulated and stuck with low emissivity films for the interior walls. For the other 4 sidewalls, high emissivity films were covered on the aluminium alloy. The cubic building simulants with 8 cm side lengths were assembled with glass slides (3 mm thick). A data logger (NI-9213, National Instruments) was used to record the temperature data of the building simulants. A PID (Proportional-Integral-Derivative) temperature controller (E5CC-QX2ASM-802, OMRON) was utilized to control the polyimide insulated flexible heater (12 Ω) to maintain the building simulant stable at 25 ℃ in the 5 ℃ ambient test. An oscilloscope (InfiniiVision DSOX4022A,

Keysight) was used to record the voltage and power supply for the heater.

Colored LE-PCC: The selected pigment nanoparticles (Prussian blue, Fe_2O_3, and goethite) for the corresponding color were dispersed in absolute ethanol with the assistance of magnetic stirring and sonication. The nanoparticle solutions were loaded into a spray gun and sprayed onto the pristine white LE-PCC. By adjusting the spray speed and spray times, the desired mass loading of pigments could be achieved after the evaporation of the ethanol.

Energy-saving calculation: We used a reference building model (post-1980 midrise apartment) defined by the US Department of Energy in EnergyPlus version 8.7. Internal gains and HVAC systems have been comprehensively designed in the models. We present 7 representative cities worldwide (Hong Kong, Los Angeles, Miami, Rio, Rome, Cairo, and Sydney) to analyze the energy-saving performance in regions across different climate zones. The baseline HVAC energy use, including cooling, heating, and fans, was calculated for the building model with conventional wall and roof properties. The initial R_{solar} values of the building exterior wall, interior wall, and roof are 0.22, 0.08, and 0.3, respectively, and MIR emissivity (thermal absorbance) values are all 0.9. To calculate the HVAC energy use with the installation of our LE-PCC, we modified the optical properties of the wall and roof surfaces (both inside and outside sides) in the building model using experimentally measured data. Comparing the energy use difference between building models with and without LE-PCC installation, we obtained the all-year energy saving for cooling, heating, fans, and total HVAC.

CRediT authorship contribution statement

Yi Zhang: Writing – original draft, Investigation, Conceptualization. **Senji Li:** Conceptualization. **Yucan Peng:** Formal analysis. **Chenglong She:** Data curation. **Minghao Dong:** Investigation. **Keqiao Li:** Methodology. **Fan Yang:** Investigation. **Weiying Hou:** Investigation. **Han Gao:** Investigation. **Chenshu Wu:** Investigation. **Baoling Huang:** Methodology. **Jiawei Zhou:** Formal analysis. **Philip C.Y. Chow:** Supervision. **Xiaobo Yin:** Writing – review & editing, Supervision.

Declaration of competing interest

The authors declare that they have no known competing financial interests or personal relationships that could have appeared to influence the work reported in this paper.

Acknowledgements

X. Y. acknowledges support from the New Cornerstone Science Foundation through the XPLORER Prize; the Hong Kong Jockey Club Charities Trust; the Hong Kong Research Grants Council through Grant No. C5051-22GF; and the Hong Kong Research Grants Council through Grant No. 17206724. P.C.Y.C acknowledges support from the Hong Kong Research Grants Council (Grant No. 17300023) and NSFC Excellent Young Scientist Fund (27200822). Y. P. acknowledges support from the National Natural Science Foundation of China (Grant No. 22475007).

Appendix A. Supplementary data

Supplementary data to this article can be found online at https://doi.org/10.1016/j.mattod.2025.10.014.

Data availability

Data will be made available on request.

References

[1] M. González-Torres, et al., A review on buildings energy information: Trends, end-uses, fuels and drivers, Energy Rep. 8 (2022) 626–637.
[2] D. Ürge-Vorsatz, et al., Heating and cooling energy trends and drivers in buildings, Renew. Sustain. Energy Rev. 41 (2015) 85–98.
[3] X. Liu, et al., Transparent ultrahigh-molecular-weight polyethylene/MXene films with efficient UV-absorption for thermal management, Nat. Commun. 15 (2024) 3076.
[4] X. Liu, et al., A transparent polymer-composite film for window energy conservation, Nano-Micro Letters 17 (2025) 151.
[5] A.P. Raman, et al., Passive radiative cooling below ambient air temperature under direct sunlight, Nature 515 (2014) 540–544.
[6] Y. Zhai, et al., Scalable-manufactured randomized glass-polymer hybrid metamaterial for daytime radiative cooling, Science 355 (2017) 1062–1066.
[7] Y. Zhang, et al., Ultrahigh performance passive radiative cooling by hybrid polar dielectric metasurface thermal emitters, Opto-Electronic Advances 7 (2024), 2301941.
[8] S. Wang, et al., A versatile strategy for concurrent passive daytime radiative cooling and sustainable energy harvesting, Small 20 (2024) 2305706.
[9] Y. Peng, et al., Colorful low-emissivity paints for space heating and cooling energy savings, Proc. Natl. Acad. Sci. 120 (2023) e2300856120.
[10] M.A. Medina, A Comprehensive Review of Radiant Barrier Research Including Laboratory and Field Experiments, ASHRAE Trans. (2012) 118.
[11] Y. Peng, et al., Coloured low-emissivity films for building envelopes for year-round energy savings, Nat. Sustainability 5 (2022) 339–347.
[12] L. Aditya, et al., A review on insulation materials for energy conservation in buildings, Renew. Sustain. Energy Rev. 73 (2017) 1352–1365.
[13] B.P. Jelle, S.E. Kalnæs, T. Gao, Low-emissivity materials for building applications: a state-of-the-art review and future research perspectives, Energ. Buildings 96 (2015) 329–356.
[14] P. Principi, R. Fioretti, Thermal analysis of the application of pcm and low emissivity coating in hollow bricks, Energ. Buildings 51 (2012) 131–142.
[15] D.E. Abraham, et al., Efficient outdoor thermal comfort via radiant cooling and infrared-reflective walls, Nat. Sustainability (2025).
[16] Z. Shi, X. Zhang, Analyzing the effect of the longwave emissivity and solar reflectance of building envelopes on energy-saving in buildings in various climates, Sol. Energy 85 (2011) 28–37.
[17] A. Joudi, et al., Reflective coatings for interior and exterior of buildings and improving thermal performance, Appl. Energy 103 (2013) 562–570.
[18] A. Joudi, et al., Highly reflective coatings for interior and exterior steel cladding and the energy efficiency of buildings, Appl. Energy 88 (2011) 4655–4666.
[19] J. Xu, et al., Colored radiative cooling coatings using phosphor dyes, Mater. Today Nano 19 (2022) 100239.
[20] C.G. Granqvist, Transparent conductors as solar energy materials: a panoramic review, Sol. Energy Mater. Sol. Cells 91 (2007) 1529–1598.
[21] Z. Wu, et al., Scalable and Tunable PEDOT: PSS Emitter for thermal Camouflage, Adv. Opt. Mater. 12 (2024) 2301303.
[22] Z. Ke, et al., Highly conductive and solution-processable n-doped transparent organic conductor, J. Am. Chem. Soc. 145 (2023) 3706–3715.
[23] L. Mercatelli, et al., Ultra-refractory diboride ceramics for solar plant receivers, Energy Procedia 49 (2014) 468–477.
[24] Y. Li, et al., 2D Ti3C2Tx MXenes: visible black but infrared white materials, Adv. Mater. 33 (2021) 2103054.
[25] A. Asp, et al., Radio signal propagation and attenuation measurements for modern residential buildings, in: In 2012 IEEE Globecom Workshops (IEEE), 2012, pp. 580–584.
[26] M. Gustafsson, et al., Design of frequency selective windows for improved indoor outdoor communication, IEEE Trans. Antennas Propag. 54 (2006) 1897–1900.
[27] G.I. Kiani, et al., Cross-dipole bandpass frequency selective surface for energy-saving glass used in buildings, IEEE Trans. Antennas Propag. 59 (2010) 520–525.
[28] S. Tripathi, et al., Millimeter-wave and terahertz spectrum for 6G wireless, in: In 6G Mobile Wireless Networks (springer), 2021, pp. 83–121.
[29] Wu, Y., Singh, S., Taleb, T., Roy, A., Dhillon, H.S., Kanagarathinam, M.R., and De, A. (2021). 6G mobile wireless networks (Springer).
[30] Jiang, W., Zhou, Q., He, J., Habibi, M.A., Melnyk, S., El-Absi, M., Han, B., Di Renzo, M., Schotten, H.D., Luo, F.-L., et al. (2024). Terahertz communications and sensing for 6G and beyond: A comprehensive review. IEEE Communications Surveys & Tutorials.
[31] L. Yunos, et al., Frequency selective surface on low emissivity windows as a means of improving telecommunication signal transmission: a review, Journal of Building Engineering 70 (2023) 106416.
[32] M. Safari, N.P. Kherani, G.V. Eleftheriades, Multi-Functional Metasurface: Visibly and RF Transparent, NIR Control and Low thermal Emissivity, Adv. Opt. Mater. 9 (2021) 2100176.
[33] L. Liu, et al., Achieving low-emissivity materials with high transmission for broadband radio-frequency signals, Sci. Rep. 7 (2017) 4840.
[34] M. Schöttle, et al., A continuous gradient colloidal glass, Adv. Mater. 35 (2023) 2208745.
[35] P.D. García, R. Sapienza, C. López, Photonic glasses: a step beyond white paint, Adv. Mater. 22 (2010) 12–19.
[36] J. Mandal, et al., Hierarchically porous polymer coatings for highly efficient passive daytime radiative cooling, Science 362 (2018) 315–319.
[37] K. Lin, et al., Hierarchically structured passive radiative cooling ceramic with high solar reflectivity, Science 382 (2023) 691–697.
[38] T. Li, et al., A radiative cooling structural material, Science 364 (2019) 760–763.

[39] Y.-L. Liu, et al., Preparation and Characterization of SiO2/α-Al2O3 Tritium Permeation Barriers at Low Temperature, Adv. Eng. Mater. 25 (2023) 2100947.
[40] Y. Roh, et al., Highly improved thermal stability of the ceramic coating layer on the polyethylene separator via chemical crosslinking between ceramic particles and polymeric binders, Chem. Eng. J. 433 (2022) 134501.
[41] H.-H. Tang, M.-L. Chiu, H.-C. Yen, Slurry-based selective laser sintering of polymer-coated ceramic powders to fabricate high strength alumina parts, J. Eur. Ceram. Soc. 31 (2011) 1383–1388.
[42] L. Cai, et al., Temperature regulation in colored infrared-transparent polyethylene textiles, Joule 3 (2019) 1478–1486.
[43] H. Zhu, et al., Multispectral camouflage for infrared, visible, lasers and microwave with radiative cooling, Nat. Commun. 12 (2021) 1805.